RESEARCH ARTICLE
•Arch Hyg Sci 2021;10(1):1-10
•Journal Homepage: http://jhygiene.muq.ac.ir

Photocatalytic Degradation of Dye Pollutant in Synthetic Wastewater by Nano-Fe_3O_4 Based on Clinoptilolite Zeolite

Maryam Sabonian[a*], Kazem Mahanpoor[b]

[a] Young Researchers and Elite Club, Arak Branch, Islamic Azad University, Arak, Iran
[b] Department of Chemistry, Arak Branch, Islamic Azad University, Arak, Iran

***Correspondence** should be addressed to Dr Maryam Sabonian, Email: m-sabonian92@iau-arak.ac.ir

A-R-T-I-C-L-EI-N-F-O

Article Notes:
Received: Jul 24, 2019
Received in revised form:
Nov 15, 2020
Accepted: Nov 16, 2020
Available Online: Dec 14, 2020

Keywords:
Alcohols
Box-behnken design
Clinoptilolite zeolite
Environmental pollutants
Fe_3O_4
Nanoparticles
Water decolorization

A-B-S-T-R-A-C-T

Background & Aims of the Study: One of the most important environmental pollutants in the alcohol industry is sugar beet molasses. The wastewater of these industries causes the pollution of soil, surface water, and underground water. Iron oxide magnetic nanoparticles have attracted much consideration due to their unique properties, such as superparamagnetism, surface-to-volume ratio, greater surface area, and easy separation methodology. Accordingly, clinoptilolite zeolite has been used due to the low cost and abundance. The purpose of this study was to remove organic and dye pollutants from the wastewater using a new catalyst that can be separated from aqueous solution by magnetic methods and take a step toward the preservation of the environment.

Materials and Methods: In this study, a new catalyst was prepared by supporting magnetite (Fe_3O_4) on clinoptilolite zeolite, and the characterization of this catalyst was studied by using scanning electron microscopy images, X-ray diffraction patterns, and nitrogen adsorption/desorption.

Results: The experiments were performed in different operational conditions, such as the amounts of photocatalyst and pH. The mathematical equation for estimating the percentage of dye pollutant removal was obtained using the Box-Behnken experimental design. The optimal conditions were determined as the amount of photocatalyst equal to 200 mg L^{-1}, pH equal to 2, and concentration of H_2O_2 equal to 25 ppm. Removal efficiency in the optimal condition was reported as 85.10%.

Conclusion: The obtained results of the present study showed that the photocatalytic process can be suitable for the removal of dye pollutants from the alcohol industrial wastewater using the supported Fe_3O_4 nanoparticles on zeolite clinoptilolite.

Please cite this article as: Sabonian M, Mahanpoor K. Photocatalytic Degradation of Dye Pollutant in Synthetic Wastewater by Nano-Fe_3O_4 Based on Clinoptilolite Zeolite. Arch Hyg Sci 2021;10(1):1-10

Background

The remediation of wastewater polluted by nitro phenols through traditional methods is really complicated and costly, producing secondary pollution and taking a long reaction time. In addition, phenol derivatives are chemically resistant based on high solubility and constancy in water (1, 2). Therefore, it is vital to adopt new approaches for the treatment of the wastewater containing these pollutants without the above-mentioned problems.

Advanced oxidation processes (AOPs) are active and ecologically friendly approaches that can degrade the organic contaminants that are resilient to the conservative treatment systems into modest byproducts and lastly mineralize them into carbon dioxide and water (3, 4). The oversensitive and general oxidant and hydroxyl radicals with high electrochemical oxidation potential were formed by AOPs (5, 6).

Heterogeneous photocatalytic techniques are usually used for the treatment of wastewater containing refractory organic pollutants with the purpose of reusing due to its ability to attain the complete mineralization of the compounds under mild conditions, such as ambient temperature and pressure. Numerous solid semiconductor metal oxides (e.g., TiO_2, CeO_2, ZnO, ZrO_2, V_2O_5, WO_3, and Fe_2O_3) and sulfides (e.g., CdS and ZnS) have been employed for the degradation of chemical substances (7-9).

Environmental obstacles in beet molasses fermentation manufacturing are principally related to the production of large quantities of polluted and brown colored sewages known as vinasse. The ultimate products of the Maillard reaction, mainly melanoidins, are part of the vinasse combination. Melanoidins are brown nitrogenous polymers with a mainly unknown structure, mostly constructed from sugar decomposition products (10). Magnetite (Fe_3O_4) is an ideal applicant for biological usages, such as drug delivery, cell separation, and magnetic-resonance imaging, due to its specific magnetic virtues, low poisoning, and good bio adaptability (11). Among the nanoparticles of metal, iron nanoparticles have been more widely considered for frequent, inexpensive, non-toxic, and rapid reaction and high ability and efficiency in the adsorption of pollutants and removal of heavy metals from contaminated waters.

Natural zeolites are becoming more and more significant for the removal of pollutant substances, such as heavy metals, due to their capacity for ion exchange, adsorption, and selectivity, in addition to thermal and mechanical properties (12). Clinoptilolite, mordenite, and phillipsite are instances of natural zeolites. Natural clinoptilolite depends on the heulandite family, with a chemical formula of $Na_6[(AlO_2)_6(SiO_2)_{30}].24H_2O$ (13). The ratio of silicon to aluminum in the context of clinoptilolite is within the range of 4-5.3. However, the ion exchange capacity of clinoptilolite is lower than that of other zeolites.

Usually, clinoptilolite zeolite can be ion-exchanged with cations, such as Na, K, Ca, and Mg (13). Due to the physical and chemical properties of zeolites, they are relatively diverse compounds. Therefore, clinoptilolite zeolite has been widely considered due to its special spatial structure, chemical stability, low cost, natural, non-recyclable, and environmentally friendly features, and wide distribution in the world (14).

In order to optimize a process, such as the removal of dye pollutant process, it is essential to study all factors influencing the process. Nonetheless, perusing the effects of individual factors on the process is difficult and time-consuming, particularly if these factors are not independent and affect each other. Using an experimental design could remove these difficulties owing to the interaction effects of various factors that could be obtained using only the Design of Experiments.

The Box-Behnken design which is the most popular experimental design style was employed to optimize the process factors (15-18) due to fewer runs. The Box-Behnken design technique has demonstrated to be a very noteworthy instrument, allowing the precise optimum values of experimental factors to be specified and feasibility to appraise the interaction between variables with a reduced number of experiments (16, 17). The analysis of the experiment was accomplished using Minitab statistical software (version 18). Multiple regression analysis was utilized to analyze the experimental data and correlation coefficients (R^2). In addition, interaction and quadratic terms were appraised through analysis of variance (ANOVA). Generally, a second-order model is used in response surface methodology (19, 20).

$$y = \beta_0 + \sum_{i=1}^{k}\beta_i x_i + \sum_{i=1}^{k}\beta_{ii} x_i^2 + \sum_{i=1}^{k-1}\sum_{j=2}^{k}\beta_{ij} x_i x_j + \varepsilon \quad (1)$$

In this model, y represents the dependent variable; β_0 is a constant value; β_i, β_{ii}, and β_{ij} refer to the regression coefficients for the linear, second-order, and interactive effects, respectively; x_i and x_j are the independent variables; ε is a random error. The β coefficients, which should be quantified in the second-order model, are obtained by the method of least squares. Generally, equation 1 can be written in matrix form as follows:

$$y = \beta X + \varepsilon \quad (2)$$

where y can be defined as a matrix of measured values, and X is a matrix of independent variables. In general, the β and ε matrixes consist of coefficients and errors, respectively.

Aims of the study

The purpose of this study was to use a clinoptilolite zeolite as a base for the stabilization of Fe_3O_4 photocatalyst and identification. In this study, the Box-Behnken design was used to appraise the effect of process parameters on the removal of dye pollutants. Factors and responses were defined as experimental variables that can be changed self-sufficiently of each other and measured value of the results of trials, respectively.

Materials & Methods

Materials

Iron(II) chloride ($FeCl_2$), Iron(III) chloride ($FeCl_3$), urea, acetone, ethanol, clinoptilolite zeolite, and hydrogen peroxide were purchased from The Merck Group (Germany).

Procedure of catalyst production

At first, about 4.72 g of $FeCl_3$ with 1.72 g of $FeCl_2$ were mixed, and then 50 g of urea $CO(NH_2)_2$ and 100 ml of distilled water were added. The balloon was then filled with nitrogen and placed above the condenser. The solution was closed by the reflux system and placed on top of the hot water bath at 90°C for 2 h. The precipitate was composed at the bottom of the container and washed with distilled water to reach a neutral pH. Finally, it was washed with an organic solvent, such as acetone (C_3H_6O), and dried at 80°C for 2 h. Subsequently, 6 g of clinoptilolite zeolite powder with 2 g of synthesized iron oxide were add in a mortar and pestle in addition to some ethanol. Then, it was shed for 30 min after drying in a furnace at 300°C for 4 h.

General procedure

In this study, according to Figure 1, iron oxide magnetic nanoparticles were stabilized on clinoptilolite zeolite, and then a dye pollutant solution was added. The suspension of nanoparticles was organized after regulating the pH under ultrasonic waves. Then, the suspension was provided within three rotary photoreactors, including a quartz tube. The solution was passed over a quartz tube and condenser, and the temperature was controlled by a thermo bath. After equilibrium, the solution was subjected to hydrogen peroxide

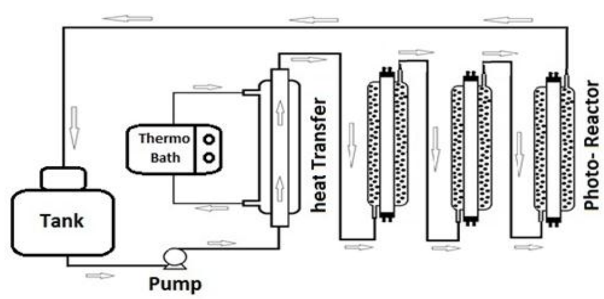

Figure 1) Schematic of laboratory photoreactor for catalytic process

and ultraviolet light to remove the dye pollutant; afterward, it was sampled at a certain interval. The regulation of pH was performed through the least use of H_2SO_4 and NaOH solution. The concentration of dye pollutants in the samples was determined using an ultraviolet-visible (UV-Vis) spectrophotometer at λ_{max} of 268 nm.

Box-Behnken experimental design

Table 1 shows the relations between the coded and original values. The effects of the reaction of pH, catalyst dosage, and H_2O_2 concentration on the percentage of dye pollutant removal were investigated. All the variables were evaluated at three levels, namely low, middle, and high. The low, middle, and high levels of each factor were chosen as −1, 0, and +1, respectively.

The number of experiments obtained using the Box-Behnken model was determined as follows:

$$N = 2K\,(K-1) + C_0 \tag{3}$$

where N is the number of the experiments; K is the number of the factors; C_0 is the number of the central points [21]. Table 2 tabulates the details of the performed Box-Behnken design of the experiment. The design presented 15 experimental runs, which were randomized to maximize the effects of unfamiliar variability in the apperceive responses owing to extraneous factors.

Effects of experimental parameters on specific surface area of samples:

The ANOVA is a collection of several statistical methods used in the analysis of the distinction between the mean of groups and related methods. The ANOVA is employed to test the significance of the mean of three or more of the three variables. In addition, this method is used for graphical data analysis to determine the interaction between process

Table 1) Factors and values of the levels for the experimental design

Design	Level	Catalyst amount (mg L^{-1})	pH	Initial concentration of H_2O_2 (ppm)
Box-Behnken	-1	100	2	20
	0	150	3	25
	+1	200	4	30

Table 2) Experimental conditions for photocatalytic process

Run	Catalyst amount (mg L^{-1})	pH	Initial concentration of H_2O_2 (ppm)	Experimental responses (%)	Predicted responses (%)
1	150	2	30	47.03	47.67
2	100	4	25	68.45	66.99
3	200	3	20	80.43	81.42
4	200	2	25	85.10	86.2
5	200	4	25	66.58	67.42
6	100	2	25	41.21	42.51
7	100	3	20	62.83	63.49
8	150	4	30	69.36	69.91
9	150	3	25	64.49	64.96
10	150	2	20	77.58	78.4
11	100	3	30	46.82	48.01
12	200	3	30	71.26	72.21
13	150	4	20	63.98	63.87
14	150	3	25	64.49	64.96
15	150	3	25	64.49	64.96

variables and response. The quality of the polynomial model is expressed through the coefficient of determination of R^2, and the significance of the coefficients is determined using F-test (Fisher's test). The components of the model are evaluated through a p-value.

Table 3 tabulates the coefficient of each of the parameters and other characteristics in the mathematical model. The model equations were obtained for the percentage of dye pollutant removal in equation 1, respectively. Based on equation 4, it can be observed that a positive value represents an effect favoring the optimization; however, a negative value indicates an inverse relationship between the factor and response. Table 4 shows the ANOVA analysis of the Box-Behnken experimental design. The correlation coefficient (R^2) is used to check the precision of a model. The p-values were less than 0.05 (22).

$$R\% = 64.967 + 10.533\,[Fe_3O_4/CZ] + 1.926\,[pH] - 6.174\,[H_2O_2] + 1.318\,[Fe_3O_4/CZ \times Fe_3O_4/CZ] - 11.315\,[Fe_3O_4/CZ \times pH] + 1.570\,[Fe_3O_4/CZ \times H_2O_2] + 9.192\,[pH \times H_2O_2] \quad (4)$$

The value of R^2 was an index for the measurement of the range of variability in the observed response. The obtained results indicated that this model had a correlation coefficient of R^2 equal to 0.9989. The value of R^2 showed that 99.89% of the changes happened in the efficiency of reduction by the independent variables. The model was ineffective to account for only 0.11% of the changes.

Further parity plot (Figure 2) illustrates a good correlation between the experimental and predicted values indicating that the model can predict the response with adequate precision.

Table 3) Coefficient of each parameter in mathematic model

Term	Coefficient	Standard error coefficient
Constant	64.967	0.213
Fe_3O_4/CZ	10.533	0.199
pH	1.926	0.199
H_2O_2	-6.174	0.199
Fe_3O_4/CZ × Fe_3O_4/CZ	1.318	0.291
Fe_3O_4/CZ × pH	-11.315	0.281
Fe_3O_4/CZ × H_2O_2	1.570	0.281
pH × H_2O_2	9.192	0.281

CZ: Clinoptilolite zeolite

Table 4) Analysis of variance results of three factorial Box-Behnken experimental designs for dye pollutant removal

Source	DF	Adjusted SS	Adjusted MS	F-value	P-value
Model	7	2088.54	298.363	941.49	0.000
Linear	3	1222.07	407.353	1285.42	0.000
Fe_3O_4/CZ	1	887.47	887.468	2800.41	0.000
pH	1	29.68	29.684	93.67	0.000
H_2O_2	1	304.92	304.922	926.18	0.000
Square	1	6.48	6.484	20.46	0.003
Fe_3O_4/CZ × Fe_3O_4/CZ	1	6.48	6.484	20.46	0.003
2-way interaction	3	895.98	286.662	904.56	0.000
Fe_3O_4/CZ × pH	1	512.12	512.117	1615.99	0.000
Fe_3O_4/CZ × H_2O_2	1	9.86	9.860	31.11	0.001
pH × H_2O_2	1	338.01	338.008	1066.59	0.000
R-squared=99.89%		R-squared (adjusted)=99.79%		R-squared (predicted)=99.48%	

CZ: Clinoptilolite zeolite

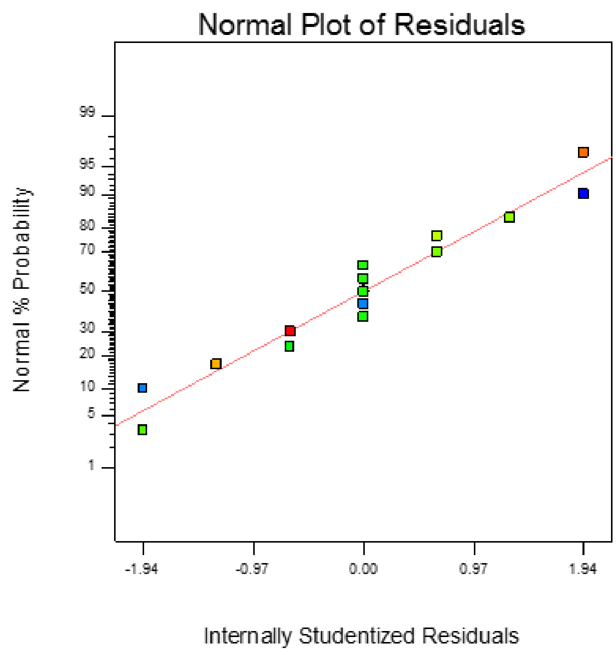

Figure 2) Correlation graph between predicted and experimental yield values

Results

X-ray diffraction analysis

X-ray diffraction (XRD) is one of the most significant characterization tools employed in solid-state chemistry and materials science. The crystallographic structure of the synthesized products was recognized by XRD measurement. Figure 3 depicts the XRD pattern of Fe_3O_4 and Fe_3O_4/clinoptilolite zeolite. No hematite peaks, metal hydroxides, or other impurities were indicated, thereby affirming the complete formation of Fe_3O_4. The strong and sharp peaks showed that Fe_3O_4 nanoparticles were of high purity and well crystalline. The average crystallite size of Fe_3O_4 nanoparticles was calculated by the Debye Scherrer formula (23).

$$L = \frac{0.89\lambda}{\beta \cos\theta} \quad (5)$$

where L is the crystallite size; λ is the X-ray wavelength; θ is the Bragg diffraction angle; β is the full width at half maximum. The average crystallite size of Fe_3O_4 nanoparticles supported on the surface of clinoptilolite zeolite was reported as 34 nm.

Scanning electron microscopy studies:

Figure 4 displays the representative micrograph morphology and structure of Fe_3O_4-CZ. As shown in the scanning electron microscopy (SEM) image, clinoptilolite zeolite is formed as different sized plates on which Fe_3O_4 nanoparticles are distributed, and the distribution of iron oxide particles is non-uniform. Cavities are observed at the catalyst level, which can increase the level of the catalyst. These cavities do not have the same dimensions, and the accumulation of iron oxide nanoparticles in the cavity openings is higher. Furthermore, in addition to crystalline parts, sections are also observed as amorphous;

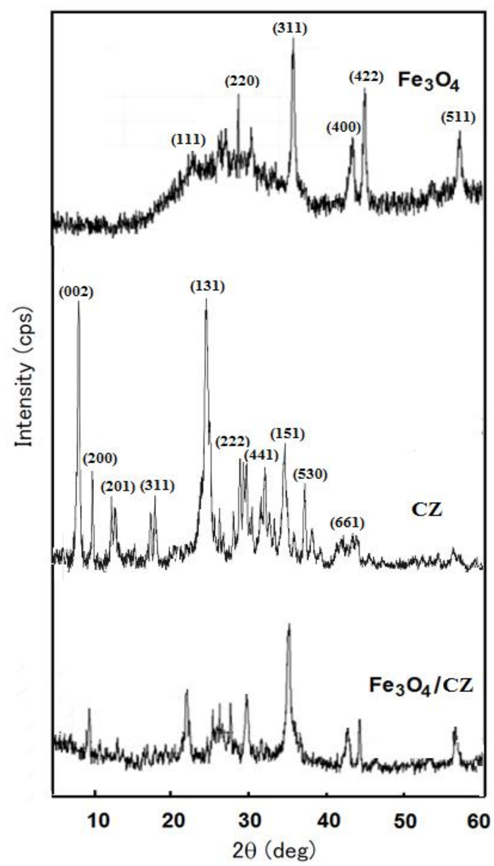

Figure 3) X-ray diffractograms of synthesized Fe_3O_4, clinoptilolite zeolite (CZ), and synthesized Fe_3O_4/CZ

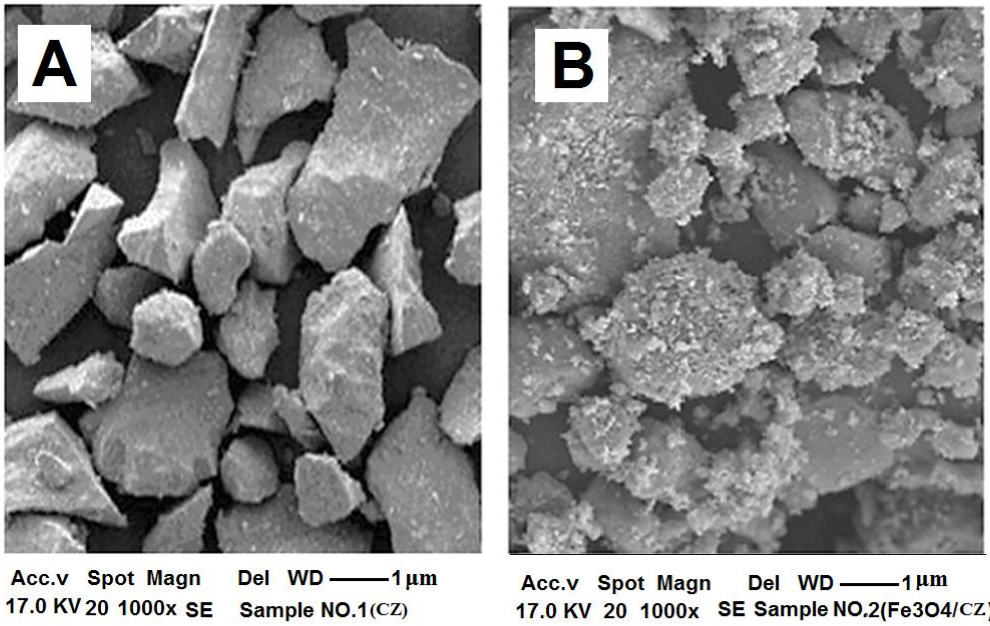

Figure 4) Results of scanning electron microscopy image of A) clinoptilolite zeolite (CZ) and B) Fe_3O_4/CZ

however, at high temperatures, small parts appear to be observed at the catalyst level as hollow accumulation.

Optical properties by Diffuse Reflectance Spectroscopy studies

The optical possessions of Fe_3O_4 nanoparticles are inspected by UV-Vis Diffuse Reflectance Spectroscopy (DRS). The assessed bandgap of Fe_3O_4 is 2.12 eV for Fe_3O_4/CZ. The isothermal adsorption/desorption curve for Fe_3O_4/CZ appears as a hysteresis loop of H_3 type with a typical two-dimensional-lamellar structure in accordance with the International Union of Pure and Applied Chemistry type IV template. The sharp increases in N_2 adsorption happened at relative pressures of 0.64-0.93 (Figure 5A). The hysteresis loops of the N_2 adsorption/desorption isotherms for Fe_3O_4/CZ clearly propose delayed agglomeration and desorption. The results of the Brunauer-Emmett-Teller (BET) surface area, volume, and pore diameter for Fe_3O_4/CZ are shown in Figure 5B and Table 5. The information in Table 5 tabulates the N_2 adsorption/desorption isotherm and pore size distribution of the nanoparticle.

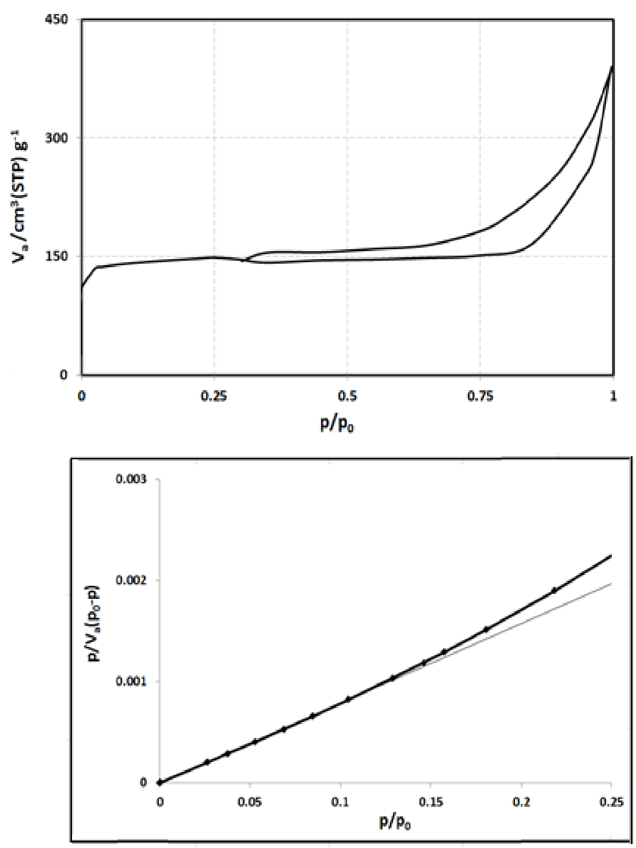

Figure 5) A) N_2 adsorption/desorption isotherms and B) Brunauer-Emmett-Teller of synthesized Fe_3O_4/clinoptilolite zeolite

Table 5) Brunauer-Emmett-Teller surface area,

volume, and pore size for Fe_3O_4/clinoptilolite zeolite

Parameter	Value
BET specific surface area (a_{sBET})	617.1 $m^2\ g^{-1}$
Monolayer volume (V_m)	135.4 cm^3 (STP) g^{-1}
Total pore volume (V_p)	0.6053 $cm^3\ g^{-1}$
Mean pore diameter (d_p)	68.27 nm

BET: Brunauer-Emmett-Teller

Based on Barrett-Joyner-Halenda's theory, the analysis of BET demonstrated that the mean surface area, total pore volume, and mean pore diameter of the present nanoparticle was 617.1 m^2/g, 0.6053 cm^3/g, and 68.27 nm, respectively.

Effects of influential variables on dye removal

Figure 6 illustrates the effect of the amount of photocatalyst and initial concentration of H_2O_2 of the solution on dye pollutant in the percentage of alcohol industrial wastewater. Figure 6 depicts the fact that with the increase for photocatalyst, the percentage of dye pollutant removal increases. The tests were performed in the darkness, and only a limited amount of dye pollutant was adsorbed on the surface of the catalyst; however, the main part of the reaction started while irritation. The reason for the increase in dye pollutant removal

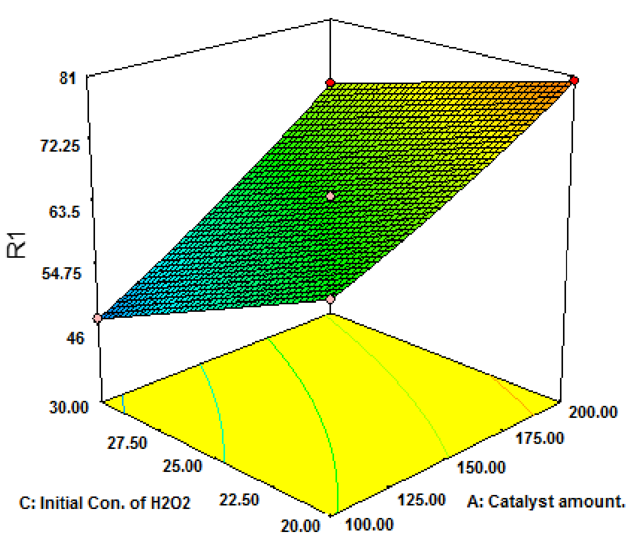

Figure 6) Three-dimensional response surface plots illustrating effect of amount of photocatalyst and initial concentration of H_2O_2 on dye pollutant removal efficiency

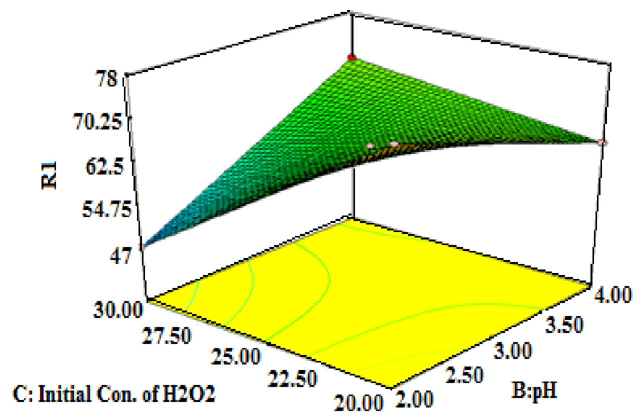

Figure 7) Three-dimensional response surface plots showing the effect of initial concentration of H_2O_2 and pH on dye pollutant removal percentage

was related to increasing the amount of photocatalyst to increase the available active centers. Moreover, by increasing the amount of photocatalyst, there is an increase in the surface area of the catalyst for adsorption leading to the absorption of pollutants (24, 25).

Discussion

The term R1 in all figures represent the removal percent of pollutant. Figure 7 shows the effect of the concentration of H_2O_2 and pH of the solution on the percentage of dye pollutant removal. By an increase in the concentration of hydrogen peroxide, the conversion rate of the photocatalytic degradation reaction reduced due to the increase in the concentration of hydrogen peroxide. This is due to the fact that hydrogen peroxide acts as a destroyer of hydroxyl radicals and it is competitively used for dye substances, causing the production of less reactive radicals of prehydroxyl ($HO_2^{\bullet}$). As shown in Figure 7, for dye pollutants, as the pH lowers, the effect of the photocatalytic process increases due to the following reactions in the acidic environment, which leads to the production of active radicals (26).

$$e_{CB} + O_{2(ads)} \rightarrow O_{2(ads)}^{\bullet} \quad (6)$$

$O_{2(ads)}^{\bullet} + H^{+} \rightarrow HO_2^{\bullet}$ (7)

$2HO_2^{\bullet} \rightarrow O_2 + H_2O_2$ (8)

$H_2O_2 + O_{2(ads)}^{\bullet} \rightarrow OH^{\bullet} + OH + O_2$ (9)

Conclusion

The present study investigated the practicability of organic and dye pollutants to be removed from the wastewater by Fe_3O_4/CZ nanoparticle as an efficient photocatalyst. Based on the results of XRD, SEM, and DRS, it was observed that Fe_3O_4 nanoparticles were decorated on the surface of clinoptilolite zeolite. The AOPs (e.g., Fe_3O_4/clinoptilolite zeolite and UV/H_2O_2) as solution-based methods were used to examine the removal of dye pollutants in the synthetic wastewater. The results of the statistical analysis indicated that the model used in this study was significantly reliable and valid. The optimal conditions were determined as the amount of photocatalyst equal to 200 mg L^{-1}, pH equal to 2, and concentration of H_2O_2 equal to mg L^{-1}. Removal efficiency in the optimal condition was reported as 85.10%. The results of the photocatalysis test showed that the removal efficiency appeared to reach 85.10%. The heterogeneity and recyclability of the photocatalyst system, along with the proper efficiency of the catalyst, are considered the most important features of the synthesized catalyst.

Footnotes

Acknowledgements

The authors would like to express their gratitude to the Young Researchers and Elite Club, Arak Branch, Islamic Azad University, Arak, Iran, for financial support.

Conflict of Interest

The authors declare that there is no conflict of interest.

References

1. Aslam M, Ismail IM, Salah N, Chandrasekaran S, Qamar M, Hameed A. Evaluation of sunlight induced structural changes and their effect on the photocatalytic activity of V_2O_5 for the degradation of phenols. J Hazard Mater 2015;286:127-35. PMID: 25569447
2. Dhaka S, Kumar R, Lee SH, Kurade MB, Jeon BH. Degradation of ethyl paraben in aqueous medium using advanced oxidation processes: Efficiency evaluation of UV-C supported oxidants. J Clean Prod 2018;180:505-13. Link
3. Shokri A. Investigation of UV/H_2O_2 process for removal of ortho-toluidine from industrial wastewater by response surface methodology based on the central composite design. Desalin Water Treat 2017;58:258-66. Link
4. Shokri A. A kinetic study and application of electro Fenton process for the remediation of the aqueous environment containing toluene in a batch reactor. Russ J Appl Chem 2017;90(3):452-57. Link
5. Shokri A, Mahanpoor K, Soodbar D. Degradation of Ortho-Toluidine in petrochemical wastewater by ozonation, UV/O_3, O_3/H_2O_2 and UV/O_3/H_2O_2 processes. Desalin Water Treat 2015;57(35):16473-82.
6. Shokri A. The treatment of spent caustic in the wastewater of olefin units by ozonation followed by electrocoagulation process. Desalin Water Treat 2018;111:173-82. Link
7. Junwu L, Zhixiang Z, Kaihui Z, Yucheng W. Preparation and characterization of Fe^{3+}-doped nanometer TiO_2 photocatalysts. J Wuhan Univ Technol Mater Sci Ed 2006;21(3):57-60. Link
8. Sabonian M, Behnajady MA. Artificial neural network modeling of Cr(VI) photocatalytic reduction with TiO_2-P25 nanoparticles using the results obtained from response surface methodology optimization. Desalin Water Treat 2014;56(11):2906-16. Link
9. Sabonian M, Mahanpoor K. Preparation of ZnO Nano catalyst supported on todorokite and photocatalytic efficiency in the reduction of chromium (VI) pollutant from aqueous solution. Iran J Catal 2019;9(3):201-11. Link
10. Shokri A. Degradation of 2-nitrophenol from petrochemical wastewater by ozone. Russ J Appl Chem 2015;88(12):2038-43. Link
11. Peng H, Hu C, Hu J, Tian X, Wu T. Fe_3O_4@mZnO nanoparticles as magnetic and microwave responsive drug carriers. Microporous Mesoporous Mater 2016;226:140-45. Link

12. Hernández-Beltrán NA, Olguín MT. Elemental composition variability of clinoptilolite-rich tuff after the treatment with acid phosphate solutions. Hydrometallurgy 2007;89(3-4):374-8. Link
13. Arefi Pour A, Sharifnia S, NeishaboriSalehi R, Ghodrati M. Performance evaluation of clinoptilolite and 13X zeolites in CO_2 separation from CO_2/CH_4 mixture. J Nat Gas Sci Eng 2015;26:1246-53. Link
14. Shokri A, Mahanpoor K, Soodbar D. Degradation of 2-nitrophenol from petrochemical wastewater by UV/$NiFe_2O_4$/Clinoptilolite process. Fresenius Environ Bull 2016;25(2):500-8. Link
15. Kirboga S, Oner M. Application of experimental design for the precipitation of calcium carbonate in the presence of biopolymer. Powder Technol 2013; 249:95-104. Link
16. Mohadesi M, Shokri A. Treatment of oil refinery wastewater by photo-Fenton process using Box–Behnken design method: kinetic study and energy consumption. Int J Environ Sci Technol 2018; 16(11):7349-56. Link
17. Khajeh M. Application of the Box-Behnken design in the optimization of a magnetic nanoparticle procedure for zinc determination in analytical samples by inductively coupled plasma optical emission spectrometry. J Hazard Mater 2009;172(1):385-9. PMID: 19647937
18. Ferreira SL, Bruns RE, Ferreira HS, Matos GD, David JM, Brandao GC, et al. Box- Behnken design: an alternative for the optimization of analytical methods. Anal Chim Acta 2007;597(2):179-86. PMID: 17683728
19. Tafreshi N, Sharifnia S, Dehaghi SM. Box–Behnken experimental design for optimization of ammonia photocatalytic degradation by ZnO/Oak charcoal composite. Proc Saf Environ Prot 2017;106:203-10. Link
20. Ambrosio E, Lucca DL, Garcia MH, de Souza MTF, de S Freitas TKF, de Souza RP, et al. Optimization of photocatalytic degradation of biodiesel using TiO_2/H_2O_2 by experimental design. Sci Total Environ 2017;581-582:1-9. PMID: 28068642
21. Zeynolabedin R, Mahanpoor K. Preparation and characterization of nano-spherical $CoFe_2O_4$ supported on copper slag as a catalyst for photocatalytic degradation of 2-nitrophenol in water. J Nanos-tructure Chem 2017;7(1):67-74. Link
22. Shokri A, Rabiee F, Mahanpoor K. Employing a novel nanocatalyst (Mn/Iranian Hematite) for oxidation of SO_2 pollutant in aqueous environment. Int J Environ Sci Technol 2017;14(11):2485-94. Link
23. Manikandan A, Vijaya JJ, Mary JA, Kennedy LJ, Dinesh A. Structural, optical and magnetic properties of Fe3O4 nanoparticles prepared by a facile microwave combustion method. J Ind Eng Chem 2014;20(4):2077-85. Link
24. Mohseni-Bandpi A, Al-Musawi TJ, Ghahramani E, Zarrabi M, Mohebi S, Abdollahi Vahed S. Improvement of zeolite adsorption capacity for cephalexin by coating with magnetic Fe_3O_4 nanoparticles. J Mol Liq 2016;218:615-24. Link
25. Shokri A, Joshaghani AH. Using microwave along with TiO_2 for the degradation of 4-Chloro-2-nitrophenol in aqueous environment. Russ J Appl Chem 2016;89(12):1985-90. Link
26. Shokri A, Salimi M, Abmatin N. Employing photo Fenton and UV/ZnO processes for removing reactive red 195 from aqueous environment. Fresenius Environ Bull 2017;26(2-A):1560-5. Link